Available online at www.sciencedirect.com
ScienceDirect
European Journal of Mechanics B/Fluids 27 (2008) 297–308

Double layer overlap in ac electroosmosis

Siddharth Talapatra, Suman Chakraborty *

Department of Mechanical Engineering, Indian Institute of Technology, Kharagpur-721302, India

Received 2 November 2006; received in revised form 24 May 2007; accepted 12 June 2007

Available online 21 July 2007

Abstract

The frequency-dependent flow of electrolytes between pairs of parallel plate micro-electrodes is analyzed in this paper, for the cases in which electric double layers formed in vicinity of the solid boundaries may strongly interact with each other. Closed form expressions for the potential distributions are first developed under certain simplifying assumptions, depicting the interactions between the oscillating electric field and charge density distribution within the double layer. It is revealed that the impact of double layer overlap on ac electroosmotic flows turns out to be more predominant at frequencies of the order of relaxation frequency of the electrode–electrolyte system. At higher frequencies, potential drop across the double layer tends to zero, due to polarization of the electrode-solution interface, and virtually no electroosmotic flows can be obtained in such cases.

Keywords: Ac electroosmosis; Double layer overlap; Microfluidics

1. Introduction

Under the influence of an alternating electric field, electrolytes kept in between parallel plate micro-electrodes may be subjected to body forces on account of charge density distribution and the induced potential gradients. This, in turn, gives rise to a fluid flow, which can be attributed to the interaction of the tangential component of a non-uniform electric field with the induced charge in the electric double layer (EDL). Termed as ac-electroosmosis, such flows have been observed experimentally [1], and have been found to be immensely useful for electrokinetic manipulation of particles in biotechnological research. Typical applications have encompassed the characterization and separation of latex spheres [2], viruses [3], DNA and proteins [4] over submicron length scales. Mathematical models have also been postulated in recent times [5] to analyze the interactions between the oscillating electric field and the charge at the diffuse double layer on the electrodes, under a thin double layer approximation. However, in many cases, the solid–liquid interfaces (inner surfaces of the parallel plates constituting the microfluidic channel) may be sufficiently close to each other, so that their EDLs overlap and interact with each other. This may have significant consequences in terms of causing a reduction in electroosmotic velocity and inducing a peak dispersion due to a transition in nature of the velocity profiles [6]. These effects cannot be mathematically captured by employing the classical Poisson–Boltzmann equation under thin double layer approximations, since such a treatment implicitly involves incorrect

* Corresponding author.
E-mail address: suman@mech.iitkgp.ernet.in (S. Chakraborty).

0997-7546/$ – see front matter
doi:10.1016/j.euromechflu.2007.06.005

boundary conditions for a system with overlapped EDL fields. This is because of the fact that the Boltzmann equation for potential distribution effectively assumes an infinitely large aqueous phase so that electrical potential is zero and the ionic concentration is equal to the original bulk ionic concentration, in the liquid far away from the charged surface. This condition, however, cannot be satisfied with overlapped EDL fields characterized by non-zero potential values at the mid-plane, and values of the central-plane ionic concentration that differ from the original bulk ionic concentration [7]. This implies that a direct use of Boltzmann equation may result in inaccurate description of ac electroosmotic velocity fields, under overlapped EDL conditions.

With a growing emphasis on developing nano-scale fluidic systems to manipulate molecular scale transport as well as to separate and identify analytes at unprecedented low levels of sample volumes, nanofluidics has recently evolved as an emerging field of interest [8–12] in the scientific research community. The well-known phenomena of electroosmosis and streaming potentials, originated out of ionic interactions in fluidic channels, have been found to be increasingly important in the nano-scale regime, because of the larger surface to volume ratios. It is important to recognize that this shift of paradigm from the micro- to the nano-domain is not merely associated with a trivial reduction in the physical length scales, but is also accompanied with new physical effects such as the overlapping of EDLs (mentioned as above), resulting in certain non-intuitive implications of surface charge and potential on the underlying electrokinetic flow phenomena [13]. A number of research investigations have been dedicated to address the underlying implications of EDL overlap in nanochannels from theoretical considerations alone [14,15], although experimental studies in these regard have rarely been reported. With remarkable advents in nano-fabrication methodologies, however, researchers have recently explored various techniques to fabricate fluidic channels of nano-scale dimensions. For example, Lee et al. [16] developed a nanochannel fabrication technique using chemical-mechanical polishing (CMP) and thermal oxidation. With this technique, they could control the width, length, and depth of the nanochannels without the need for nanolithography. The use of sacrificial SiO_2 layers allowed them to fabricate nanochannels with axial lengths of the orders of few centimeters. Using this methodology, they could successfully fabricate an array of extremely long and narrow nanochannels with smooth inner surfaces. In a subsequent pioneering experimental investigation, Heyden et al. [17] reported the measurements of streaming currents generated in rectangular silica nanochannels down to 70 nm in height. In their experiments, nanofluidic channels were fabricated following a silicate bonding procedure, and were patterned fluidic reservoirs on a fused silica substrate by electron-beam lithography. The channels were plasma etched to the requisite hydraulic diameter in the nano-scale regime. After a thorough cleaning procedure, the channels were sealed by first spinning a 20 nm layer of sodium silicate from 2% aqueous solution onto a flat fused silica chip, and subsequently by pressing the silicate-coated surface to the patterned channel surface. The nanofluidic device was finally cured at 100 °C for 2 h. The channels were connected to a Plexiglas holder using silicone O rings, so as to form a watertight seal. Electrical connections were established by inserting a Ag/AgCl electrode through a T junction on one end of the channel, and a plain Ag/AgCl electrode wire into the liquid on the other end.

From a thorough review of literature, it is evident that the reported theoretical and experimental investigations on electrokinetic flows with overlapped EDL conditions in nanochannels have primarily concerned with the direct current (DC) electric fields only. On the other hand, it has been well recognized by the research community that alternating electric fields can be of potential importance in manipulating molecular level transport in narrow fluidic confinements. This has motivated us to investigate the consequences of EDL overlap in nanochannels under the action of time-periodic electrical fields. The present study, accordingly, is devoted to obtain solutions for the ac electroosmotic velocity field between infinitely wide parallel electrode pairs (constituting a nanofluidic confinement) under overlapped EDL conditions. First, certain practical considerations regarding the ionic advection flux are examined, leading to a decoupling of the electrical problem and the fluid flow problem. The problem of electrical potential distribution is then analyzed under the condition of overlapped EDL fields. The expression for electrical potential distribution is subsequently employed to obtain the velocity field within the parallel plates. Using the above, cases with overlapped and non-overlapped EDL fields are eventually compared, and conclusions are drawn based on the pertinent observations with regard to implications of EDL overlap on ac electroosmotic flow mechanisms.

2. Mathematical model

The model situation under investigation consists of two pairs of infinitely large plates, with an imposed alternating voltage, as depicted in Fig. 1. Distance between the two plates, $2b$, is such that their corresponding electric double

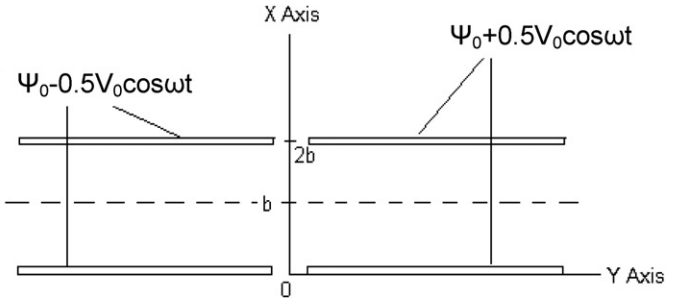

Fig. 1. A schematic diagram describing the problem domain.

layers overlap and interact with one another. The liquid phase is assumed to be a simple symmetric electrolyte solution (such as, KCl or NaCl). The fundamental electrostatic equation for the system is the Poisson's equation for electrostatic potential (ψ), which can be described as:

$$\frac{\partial^2\psi}{\partial x^2}+\frac{\partial^2\psi}{\partial y^2}=-\frac{\rho_e}{\varepsilon} \tag{1}$$

where ε is permittivity of the medium, and ρ_e is the charge density per unit volume that can be expressed as [14]

$$\rho_e = e(n_+ - n_-). \tag{1a}$$

Here n_+ and n_- represent ionic number concentration of positive and negative charges, respectively. The two ion number conservation equations are:

$$\frac{\partial n_\pm}{\partial t}+\left(\mathbf{i}\frac{\partial}{\partial x}+\mathbf{j}\frac{\partial}{\partial \gamma}\right)[\mp n_\pm\mu\nabla\psi - D\nabla n_\pm + n_\pm\mathbf{u}]=0 \tag{2}$$

where **i** and **j** are unit vectors along x and y respectively, **u** is the liquid velocity, μ is the mobility, and D is the diffusion coefficient of the ions. In Eq. (2), the last term in right hand side can be neglected, by noting that the convection current is typically much smaller than the conduction current, since ionic velocities are typically O(1 cm/s), whereas liquid velocities are about two orders of magnitude lower than that [1].

The above equations are subject to the pertinent boundary conditions, described as follows. At the electrode surfaces, the potential is equal to the sum of the static potential (ψ_0) and an applied alternating voltage of amplitude V_0, such that

$$\left.\begin{aligned}\psi &= \psi_0+\frac{1}{2}V_0\cos wt,\ \text{if } y>0\\ \psi &= \psi_0-\frac{1}{2}V_0\cos wt,\ \text{if } y<0\end{aligned}\right\}\quad \text{at } x=0,2b. \tag{3a}$$

Also, from symmetry conditions at the centerline:

$$\left.\begin{aligned}&\frac{\partial\psi}{\partial x}=0\\ &n_+=n_+^b,\quad \text{and}\quad n_-=n_-^b,\quad \text{at } y=0\end{aligned}\right\}\quad \text{at } x=b. \tag{3b}$$

In needs to be noted here that under overlapped EDL conditions, the parameters n_+^b and n_-^b are not known a-priori. In the present study, these parameters are obtained by appealing to the ionic dissociation and the pertinent mass conservation considerations, as detailed in Qu and Li [16].

Next, governing equations for the electrical field are non-dimensionalized, with the pertinent variables scaled as follows (subscript 1 refers to dimensionless variable):

$$x_1=\frac{x}{\lambda_D},\quad y_1=\frac{y}{L},\quad \psi_1=\frac{\psi e}{k_{\mathrm{B}}T},\quad \rho_{e1}=\frac{n_+-n_-}{n_+^b+n_-^b},\quad n_1=\frac{n_++n_-}{n_+^b+n_-^b},\quad t_1=t\omega. \tag{4}$$

In the above parameters, λ_D refers to the double layer thickness, and is given by

$$\lambda_D=\left(\frac{D\varepsilon}{\sigma}\right)^{1/2} \tag{4a}$$

where $\sigma = (n_+^b + n_-^b)e\mu$. Here, σ is the electrical conductivity, ω is the applied frequency, k_B is the Boltzmann constant, T is absolute temperature, μ is the mobility, and L refers to a characteristic length along the y axis. Further, five additional dimensionless parameters are defined as follows:

$$\delta = \frac{\lambda_D}{L}, \quad V_{01} = \frac{V_0 e}{k_B T}, \quad \psi_{01} = \frac{\psi_0 e}{k_B T}, \quad b_1 = \frac{b}{\lambda_D}, \quad w_1 = w\left(\frac{\varepsilon}{\sigma}\right). \tag{4b}$$

In the subsequent discussions, for notational convenience, subscripts are removed from the non-dimensional variables and parameters, leading to the following governing equations for electrical field (with an additional consideration of the relationship $k_B T/e = D/\mu$; also known as the Einstein–Smoluchowski relationship):

$$\frac{\partial^2 \psi}{\partial x^2} + \delta^2 \frac{\partial^2 \psi}{\partial y^2} = -\rho_e, \tag{5}$$

$$w\frac{\partial \rho_e}{\partial t} - \frac{\partial}{\partial x}\left\{\frac{\partial \rho_e}{\partial x} + n\frac{\partial \psi}{\partial x}\right\} - \delta^2 \frac{\partial}{\partial y}\left\{\frac{\partial \rho_e}{\partial y} + n\frac{\partial \psi}{\partial y}\right\} = 0, \tag{6}$$

$$w\frac{\partial n}{\partial t} - \frac{\partial}{\partial x}\left\{\frac{\partial n}{\partial x} + \rho_e\frac{\partial \psi}{\partial x}\right\} - \delta^2 \frac{\partial}{\partial y}\left\{\frac{\partial n}{\partial y} + \rho_e\frac{\partial \psi}{\partial y}\right\} = 0. \tag{7}$$

Eqs. (5)–(7) are subject to the following boundary conditions (in a dimensionless form):

$$\left.\begin{aligned} &\frac{\partial \rho_e}{\partial x} + n\frac{\partial \psi}{\partial x} = 0, \quad \text{for all } y \\ &\frac{\partial n}{\partial x} + \rho_e\frac{\partial \psi}{\partial x} = 0, \quad \text{for all } y \\ &\psi = \psi_0 + \frac{1}{2}V_0 \cos \omega t, \quad \text{for } y > 0 \\ &\psi = \psi_0 - \frac{1}{2}V_0 \cos \omega t, \quad \text{for } y < 0 \end{aligned}\right\} \quad \text{at } x = 0, 2b, \tag{8}$$

$$\left.\begin{aligned} &\frac{\partial \psi}{\partial x} = 0, \quad \text{for all } y \\ &\frac{\partial \rho_e}{\partial x} = 0, \quad \text{for all } y \\ &n = 1, \quad \text{for } y = 0 \end{aligned}\right\} \quad \text{at } x = b. \tag{9}$$

It can be noted here that the above-mentioned boundary conditions can be perceived as direct consequences of the following constraint: $\hat{n} \cdot \vec{J}_\pm = 0$ at the electrodes, where $\hat{n}$ is a unit vector normal to the direction of the electrodes and $\vec{J}_\pm$ represents the ionic flux. Physically, this condition originates from the fact that since the electrodes are ideally polarizable; the normal component of the ion density current vanishes at the electrodes. Resolving the boundary condition into its corresponding scalar components, one may obtain: $-n_+\mu\partial\psi/\partial x - D\partial n_+/\partial x = 0$ and $n_-\mu\partial\psi/\partial x - D\partial n_-/\partial x = 0$. Addition and subtraction of the above two equations yield the two sets of boundary conditions given by Eqs. (8) and (9), respectively.

In an effort to linearize the above system of equations for obtaining closed-form solutions, both ψ_0 and V_0 are assumed to be small. In this limit, both the electric potential and charge density turn out to be small. Accordingly, the mean ion density can be assumed to vary slightly from its value at the central symmetric location, which implies:

$$n = 1 + c \tag{9a}$$

where $c \ll 1$. Above linearization essentially renders the superposition principle applicable to decompose each function as an algebraic sum of a static (denoting subscript 's') and an oscillatory part. Thus, the static equations reduce to the following:

$$\frac{\partial^2 \psi_s}{\partial x^2} + \delta^2 \frac{\partial^2 \psi_s}{\partial y^2} = -\rho_{es}, \tag{10}$$

$$\left[\frac{\partial^2}{\partial x^2} + \delta^2 \frac{\partial^2}{\partial y^2}\right]\{\rho_{es} + \psi_s\} = 0, \tag{11}$$

$$\frac{\partial^2 c_s}{\partial x^2} + \delta^2 \frac{\partial^2 c_s}{\partial y^2} = 0 \tag{12}$$

with the pertinent boundary conditions as

$$\left.\begin{aligned} &\frac{\partial}{\partial x}(\rho_{es} + \psi_s) = 0 \\ &\psi_s = \psi_0 \\ &\frac{\partial c_s}{\partial x} = 0 \end{aligned}\right\} \quad \text{for all } y, \text{ at } x = 0, 2b, \tag{13}$$

$$\left.\begin{aligned} &\frac{\partial \psi_s}{\partial x} = 0 \\ &\frac{\partial \rho_{es}}{\partial x} = 0 \\ &c_s = 0, \text{ for } y = 0 \end{aligned}\right\} \quad \text{at } x = b. \tag{14}$$

The above system of equations can be solved by assuming each function (ψ_s, ρ_{es}, or c_s) as a product of two separable functions in x and y, respectively. This leads to the following solutions for the static problem:

$$\psi_s = \frac{\psi_0}{1 + \mathrm{e}^{2b}}\left(\mathrm{e}^{x} + \mathrm{e}^{(2b-x)}\right), \tag{15a}$$

$$\rho_{es} = -\frac{\psi_0}{1 + \mathrm{e}^{2b}}\left(\mathrm{e}^{x} + \mathrm{e}^{(2b-x)}\right), \tag{15b}$$

$$c_s = 0. \tag{15c}$$

It can be observed here that the above distribution depends only on the x coordinate (perpendicular to the flow). Moreover, since the static distribution does not produce any stress in the liquid, it turns out to be inconsequential for the subsequent part of this analysis.

For the oscillating part, complex amplitudes can be used instead of time dependent functions. Thus, for any time-dependent function of the form $\mathrm{Re}(F \exp(\mathrm{i}\omega t))$, only the amplitude F features in the equations presented below. Further, from the physical problem, it is obvious that the charge density and potential distributions are odd functions of the variable y, and hence, only one fourth of the domain will be considered ($y > 0$, $x \leqslant b$). Governing equations for the oscillating part, valid over that domain, can be stated as follows:

$$\frac{\partial^2 \psi}{\partial x^2} + \delta^2 \frac{\partial^2 \psi}{\partial y^2} = -\rho_e, \tag{16}$$

$$\mathrm{i}\omega\rho_e - \frac{\partial^2}{\partial x^2}\{\rho_e + \psi\} - \delta^2 \frac{\partial^2}{\partial y^2}\{\rho_e + \psi\} = 0. \tag{17}$$

Eqs. (16)–(17) are consistent with the following boundary conditions:

$$\left.\begin{aligned} &\frac{\partial}{\partial x}(\rho_e + \psi) = 0 \\ &\psi = \frac{V_0}{2} \end{aligned}\right\} \quad \text{at } x = 0. \tag{18a}$$

Further, from symmetry considerations at $x = b$, one may write

$$\left.\begin{aligned} &\frac{\partial \psi}{\partial x} = 0 \\ &\frac{\partial \rho_e}{\partial x} = 0 \end{aligned}\right\} \quad \text{at } x = b. \tag{18b}$$

For solution of Eqs. (16) and (17), a Fourier sine transformation can be employed, to obtain closed form expressions for the variables ρ_e and ψ in the following forms:

$$\rho_e = \int_0^\infty \left(C_1 e^{ax} + C_2 e^{-ax}\right) \sin(ky)\, dk, \tag{19}$$

$$\psi = \int_0^\infty \left(C_3 e^{k\delta x} + C_4 e^{-k\delta x} - \frac{C_1}{1+i\omega} e^{ax} - \frac{C_2}{1+i\omega} e^{-ax}\right) \sin(ky)\, dk \tag{20}$$

where $a = \sqrt{1 + i\omega + k^2\delta^2}$ and ω is a non-dimensional frequency.

By applying boundary conditions (18a–b), the constants C_1, C_2, C_3 and C_4, as appearing in Eqs. (19) and (20) can be obtained (for detailed solution, see Appendix A). Further, it can be observed here that the decoupled ion-density equation leads to a trivial solution of $c = 0$, for the dynamic problem.

It is important to note here that the stress generated by interaction of the time-harmonic electrical field and the charge density gives rise to an ac-electroosmotic flow, which is eventually opposed by viscous action. The pertinent governing equations for fluid flow, under these conditions, can be written as follows:

$$\nabla \cdot \mathbf{u} = 0, \tag{21}$$

$$\rho_f \frac{D\mathbf{u}}{Dt} = -\nabla p + \eta \nabla^2 \mathbf{u} + \rho \mathbf{E} \tag{22}$$

where ρ_f is the fluid density, η is the dynamic viscosity, and p is the pressure. The expression for the potential distribution is substituted in Eq. (22), and the resultant fluid flow equations are numerically solved by employing a pressure-based fully time-implicit finite volume method [18], to obtain the velocity distribution within the confinement. Overall, a 100×100 non-uniform rectangular grid system is chosen to discretize the problem domain, with more number of grid points being skewed adjacent to the electrodes to capture the local velocity and potential gradients. Convection–diffusion terms in the discretized governing equations are modeled by employing a Power-law [18] differencing scheme. The coupled equations of fluid flow are discretized by employing a pressure based primitive variable formulation according to the SIMPLER algorithm [18]. The resultant system of algebraic equations is iteratively solved by a line-by-line tridiagonal matrix algorithm (TDMA) solver [18]. With this method, the boundary information is quickly transmitted to the interior of the domain by direction alteration of 'sweeping', resulting in quick convergence. Also, as an aid for handling non-linearities, controlled convergence is achieved by the introduction of suitable under-relaxation parameters in the iterative scheme. The no-slip boundary condition is employed on the electrode surfaces, whereas the transverse gradient of the axial velocity component is set to zero at the symmetry plane (channel centerline). At every other boundary, the tangential velocity component is set to zero. The normal component of velocity is set to zero over all the domain boundaries.

3. Results and discussions

In order to obtain the case of dc electroosmosis as a special case of the present model, a limiting behavior of Eqs. (19) and (20) is examined, with $\omega \to 0$, and the resultant variation is depicted in Fig. 2. A comparison is also made between the present model predictions and the results obtained by employing a non-overlapped EDL theory. All curves are plotted at $y = 1$ (where y is non-dimensional distance along y-axis, the non-dimensionalizing factor being L). Figs. (2a) and (2b) pertain to two different separation distances, given by $b/\lambda_D = 0.5$ and $b/\lambda_D = 2.0$, respectively. The electrolyte concentration is taken to be 10^{-5} M and pH value of the solution is taken to be 7. Because of symmetry, only the potential distribution in the half space, i.e., from one plate surface to the middle plane, is plotted. It is observed from Fig. 2 that potential drop calculated from the present theory is sufficiently higher than that predicted by a non-overlapped EDL theory. This can be attributed to the ionic concentration distribution that differs considerably from the same under a thin EDL approximation. (Since the potential drop is directly proportional to charge density, which in turn, is directly proportional to the difference between the anion and cation concentrations.) For anions, the number concentration increases with distance from the solid surfaces, whereas, for cations, the same decreases as one moves away from the solid surface. However, absolute values of cation concentration and anion concentration always remain greater than their respective values corresponding to the original bulk solution. Moreover, the local concentration difference between anions and cations turns out to be more for the overlapped EDL case (because of stronger concentration gradients prevailing near the solid boundaries). It can also be observed that the difference

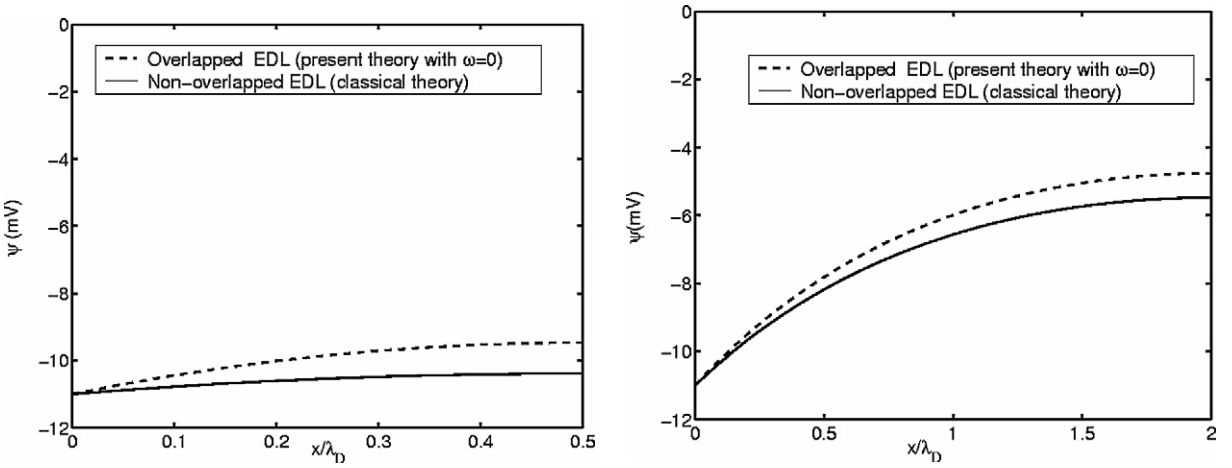

Fig. 2. A comparison with non-overlapped EDL theory, for DC electroosmosis, with (a) left panel: $b/\lambda_D = 0.5$, (b) right panel: $b/\lambda_D = 2$.

between the predictions made by the two theories turns out to be more prominent for the cases in which distance of separation between the opposite plates is made to be less. This can be attributed to the fact that the ionic concentration distribution tends to be same as that predicted by a non-overlapped EDL theory, as the opposite plates are kept at a sufficient distance apart so that respective EDLs do not interfere with each other. As such, it is revealed that for $b/\lambda_D > \mathrm{O}(10)$, the results from the overlapped and non-overlapped EDL theories turn out to be virtually identical. However, in case the distance between the two plates is kept below a threshold limit, the EDL overlap phenomenon may occur, leading to a significant deviation of the actual situation from the predictions obtained by employing a non-overlapped EDL theory. It is also important to mention here that the quantitative trends depicted in Figs. 2(a) and 2(b) are in perfect agreement with the results reported by Qu and Li [14].

Figs. 3(a) and 3(b) depict the variation of non-dimensional potential, $\psi(k_B T/e)$, as a function of scaled non-dimensional frequency, $w(\varepsilon L/(\lambda_D \sigma))$, corresponding to the separation distances given by: $b/\lambda_D = 0.5$ and $b/\lambda_D = 2.0$, respectively. From Fig. 3(b) it is observed that the potential attains a steady value at relatively higher frequencies, although non-linear variations in the potential are typical at somewhat lower frequencies. Such a behavior is in concurrence with experimental results [1] reported in the literature. Physically, this kind of a phenomenon occurs because of the fact that at lower frequencies, almost the entire potential drop takes place within the EDL, whereas at higher frequencies the potential drop across the EDL goes to zero, due to polarization of the electrode/solution interface. In between, the potential attains a maximum at an intermediate frequency, the value of which depends on the distance of

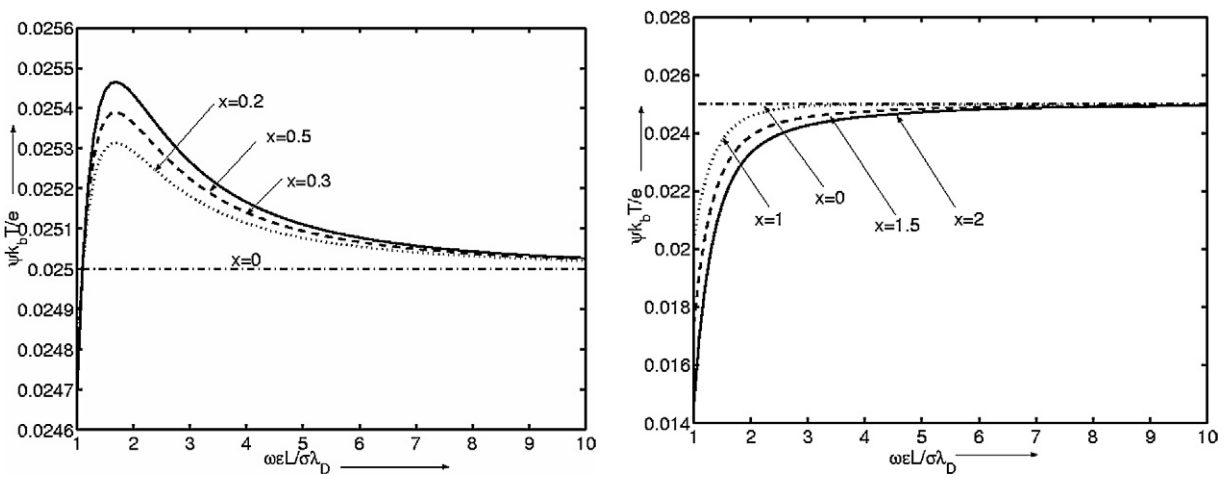

Fig. 3. Non-dimensional voltage as a function of non-dimensional frequency, with (a) left panel: $b/\lambda_D = 0.5$, and (b) right panel: $b/\lambda_D = 2$, for different values of x (non-dimensional). All curves are plotted for y (non-dimensional) $= 1$.

the specific location from either of the two plates. With a shorter distance of separation between the opposite plates, the potential gradients turn out to be stronger. From the plots obtained at different values of x, it can be seen that the maximum potential drop takes place at the center of the channel ($x = 0.5$). In fact, the potential drop increases rapidly from zero at the channel walls to non-zero values in the vicinity, and then gradually attains a local maximum value at the channel centerline. This can be explained by appealing to the physical origin of ac electroosmotic forces, as follows. The radial field established between consecutive electrodes with opposite polarities can be resolved into normal and tangential components, with respect the microchannel configuration. The tangential components of the field give rise to a Coulombic force on the fluid, which is responsible for ac electroosmosis. As one moves away from one electrode in a direction perpendicular to the same, the corresponding tangential component of the field tends to become stronger. At the centerline, the tangential component attains a local maximum, resulting in the most severe electrosmotic forces. It can be noted here that normal components of the field nullify each other, and hence do not contribute towards a net driving force for the fluid flow to occur. Further, from Fig. 3(b), a contrasting behavior in comparison to Fig. 3(a) can be observed, in a sense that the potential increases monotonically from a smaller value at the lower frequencies to a somewhat larger value at higher frequencies, before a state of saturation is reached, the corresponding asymptotic value of the potential being same as the channel wall potential. Such an asymptotic variation in the electrical potential can be attributed to the fact that this case effectively represents a situation in which, unlike the previous case, EDL overlap does not occur. As a result, the fluid elements located beyond the EDL remain rather insensitive to the charge density gradients imposed on the system near the electrode/solution interface. This insensitiveness is further aggravated by polarization of the electrode/fluid interface at relatively higher frequencies. As a consequence, a saturation state in the electrical potential is attained corresponding to a critical frequency, the threshold limit of which is somewhat lower than that observed under an overlapped EDL condition.

Figs. 4–6 depict the characteristic features of the flow-field, subject to the potential distributions described earlier. For obtaining these figures, following values of the physical parameters are considered: $V_0 = 0.5$ V, $\varepsilon = 7 \times 10^{-10}$ F/m, $\eta = 10^{-3}$ kg/m s, $\sigma = 10^{-2}$ S/m. These data are taken in accordance with the ranges of the practical demonstration experiments conducted by Green et al. [1] on the fluid flow induced by non-uniform ac electric fields in electrolytes on microelectrodes, with a vision towards exploring the sub-micrometer scale for the efficient characterization and separation of latex spheres, viruses, DNA, and proteins through ac electrokinetics. In their experiments, fluid motions were measured on microelectrode structures fabricated using microelectronic manufacturing techniques. Plate electrode pairs were fabricated on a planar glass substrate using photolithography, consisting of layers of 10-nm titanium, 100-nm gold, and 20-nm titanium. The electrodes were 2 mm long and 100 μm wide, and the gap between the electrodes could be tuned within a range of few hundreds of nanometers. The ac signals were obtained from a function generator. Different concentrations of KCl in water were used for the electrolytes, with conductivities measured using a impedance analyzer and a conductivity cell. Under such conditions, the characteristic thickness pf the EDL would solely depend on the properties of the liquid and not on any properties of the surface [14]. For example,

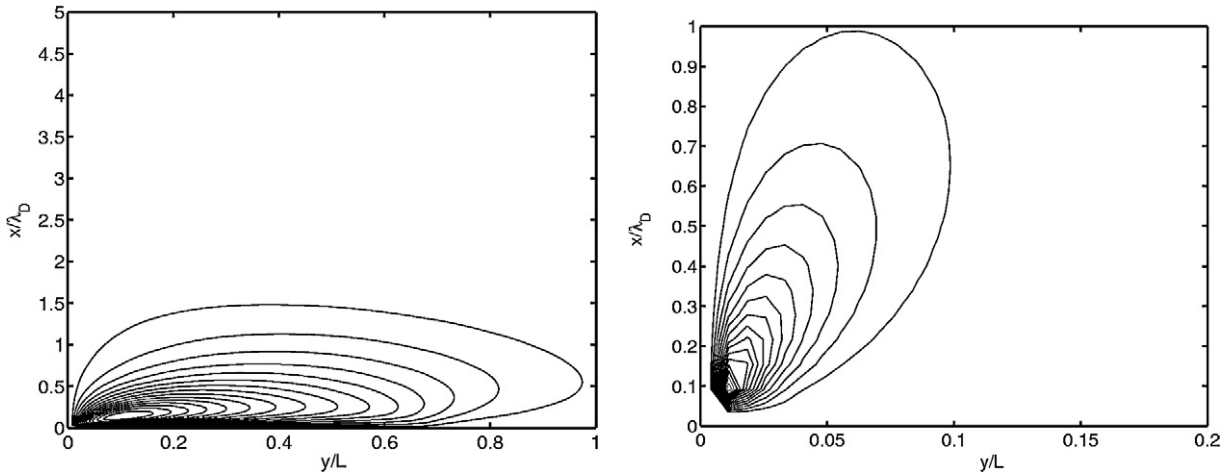

Fig. 4. Streamlines depicting the flow patterns at a frequency of 1000 Hz, for (a) left panel: $b/\lambda_D = 5$, and (b) right panel: $b/\lambda_D = 1$.

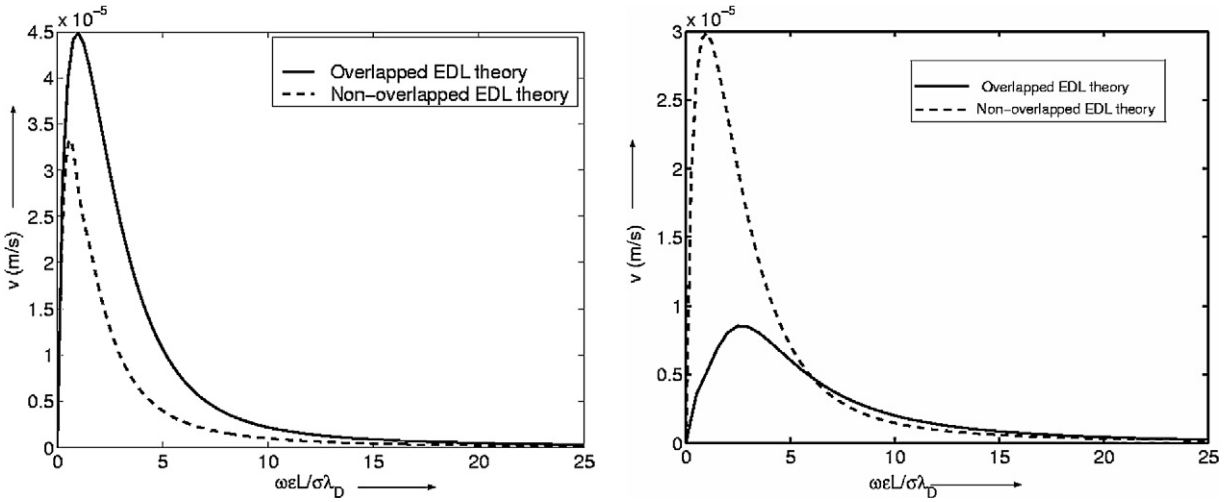

Fig. 5. Axial component of the peak flow velocity over the electrodes as a function of non-dimensional frequency, with (a) left panel: $b/\lambda_D = 0.5$, and (b) right panel: $b/\lambda_D = 2$, corresponding to y (non-dimensional) $= 0.5$.

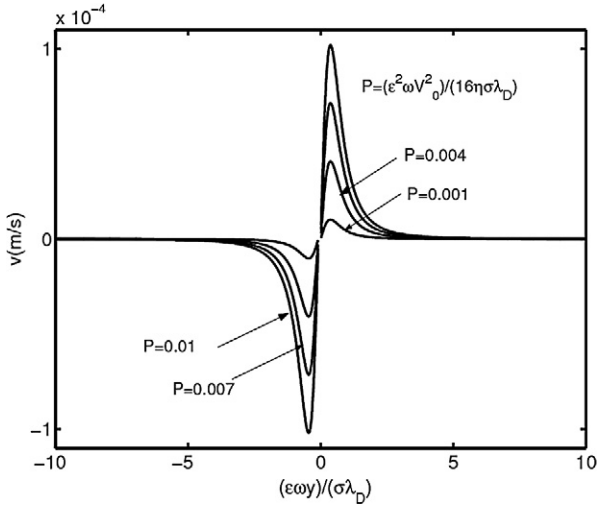

Fig. 6. Variation of flow velocity over the bottom electrodes as a function of y, with both the positive and negative electrodes taken together, for $b/\lambda_D = 0.1$.

for a 1:1 electrolyte of concentration C, $\lambda_D = 0.304/\sqrt{C}$ nm (where C is in molar units). This is estimated by taking $T = 298$ K, $\varepsilon = 78.5 \times 8.85 \times 10^{-12}$ C^2/N m^2, $e = 1.602 \times 10^{-19}$ C, $k_B = 1.38 \times 10^{-23}$ J/K and $n_0 = 1000N$, where N is the Avogadro number. Thus, for a 10^{-6}M KCl solution, $\lambda_D \approx 300$ nm. Physically, as the bulk ionic concentration decreases, less counterions are attracted to the region close to the charged surface to neutralize the surface charge. As a result, the EDL thickness is enhanced and the EDL appears to be somewhat 'stretched'. For different studies, the distances between the two opposite plates could be adjusted to the order of λ_D and even to an order lower, in order to demonstrate the consequences of the strong EDL interactions.

Fundamentally, the fluid flow in the above-mentioned configuration originates from the stress produced by the interaction between the externally applied electric field and the charge density distribution due to the induced potentials, which is balanced by viscous stresses. Both the charge density and the electric field happen to be time-oscillating harmonic functions, the product of which has a non-zero time average, leading to a continuous fluid motion. Superimposed on the static solution is an alternating motion, which originates from the coupling between the static and the dynamic solutions. With a characteristically high frequency in the tune of the applied voltage, such motions are not observable under experimental conditions [1], and hence, are not considered in this study. Because of the induced

negative charges on the positive electrode and the induced positive charges on the negative electrode, an electrical field is generated, which possesses a tangential component parallel to the electrodes. On the positive electrode, the electric field acts parallel to the positive y-direction, whereas on the negative electrode, the same acts parallel to the negative y-direction. The resultant fluid flow passes over the electrode surfaces, and eventually completes a loop that ultimately forces the liquid to flow downwards adjacent to the inter-electrode gap, in order to satisfy the requirements of continuity of the fluid motion. Thus, the axial velocities on the two electrodes are oppositely directed (towards the positive y axis on the positive electrode and towards the negative y axis on the negative electrode), giving rise to four distinct rolls in the four quadrants of the physical domain. The present analysis attempts to depict the continuous flow pattern in one such representative quadrant. Figs. 4(a) and 4(b) depict the streamlines obtained from the present analysis, for $b/\lambda_D = 5$ and $b/\lambda_D = 1$, respectively, corresponding to a frequency of 1000 Hz. Clearly, the former case represents a situation in which the EDL does not effectively penetrate into the centerline, whereas the later case represents a limiting situation in which the EDL spans upto the channel centerline. Accordingly, in the later case, the gradients in axial components of the flow velocities turn out to be prominent even at locations very close to the channel centerline. In either cases, a two-dimensional nature of the velocity field can be observed, which cannot be captured by approximate one-dimensional flow models that are routinely invoked in the literature under thin EDL limits. In order to depict the frequency dependence of flow velocities over the control electrodes, Fig. 5 is plotted. It can be observed from Fig. 5 that the maximum velocity increases as the distance of separation between the opposite plates decreases. Further, from Fig. 5(a), it can be noticed that the maximum velocity occurs at relatively lower frequencies under overlapped EDL conditions, beyond which the flow strength effectively dies down. A reasoning behind this can be put forward by following similar explanations that go with the potential distribution depicted in Fig. 3(a). Moreover, for $b/\lambda_D = 0.5$, it is observed that the overlapped EDL theory predicts higher velocities in comparison to the non-overlapped theory, for all ranges of the frequency. This can be justified from the fact that for channels with actual EDL overlaps (as for this case), appreciable velocity gradients are present throughout the entire channel section, which results in stronger electroosmotic effects and hence higher values of the peak velocity. Another observation that can be made from Fig. 5(a) is that the frequency response of the velocity dies down more sharply in accordance with the non-overlapped EDL theory, in comparison to that corresponding to the overlapped EDL theory. This may be attributed to the fact that when the EDL overlap phenomenon is not considered in the mathematical model and far-stream boundary conditions are imposed along the channel centerline, the solution of the resultant flow field is virtually insensitive to the modifications in the frequency-dependence of the charge density distributions originating out of the EDL interactions. At higher frequencies, however, the time scale of establishment of the charge distribution, or the so-called relaxation time, turns out to be so large that changes in the charge density distribution cannot effectively propagate till the centerline, and consequently, velocity characteristics obtained from the overlapped and non-overlapped EDL theories virtually coincide. For the case of $b/\lambda_D = 2.0$ (Fig. 5(b)), the EDLs do not actually overlap. Nevertheless, the overlapped EDL theory computes a transverse gradient of potential with a presumption that the same prevails till the centerline. In reality, however, at low frequencies, the entire potential drop virtually takes place within the EDL. Since the actual EDL thickness is smaller than half of the channel height in this case, the non-overlapped EDL theory correctly predicts a steeper potential gradient, especially at lower frequencies. A steeper potential gradient, in turn, implies a higher local charge density, and hence, a stronger electroosmotic body force. This results in the prediction of higher flow velocities by the non-overlapped EDL theory at lower frequencies, for the cases in which the EDL overlap does not actually occur. Fig. 6 depicts the changes in the flow velocities immediately on top of the bottom electrodes with variations in the axial coordinate, y (both the positive and negative electrodes being taken together), for $b/\lambda_D = 0.1$, as a parametric function of a combination of a number significant physical parameters, namely, $P = \varepsilon^2\omega V_0^2/(16\eta\sigma\lambda_D)$. With prominent overlapped EDL conditions, the time averaged flow velocity rapidly decays to zero, as $|w\varepsilon y/(\lambda_D\sigma)|$ approaches a threshold value of approximately 5. Regarding implications of the parameter P, it can be clearly observed that higher values of P are associated with higher peak electroosmotic flow velocities. This effectively offers with a judicious combination of the important physical parameters for achieving maximized rates of electrokinetic transport, within the constraints of a chosen electrode configuration.

4. Conclusions

Non-uniform ac electric fields across parallel plate micro- or nano-electrodes may induce an axial fluid motion, which has its origin in the interaction of the tangential component of the non-uniform field with the charge induced

within the EDL in vicinity of the electrode surfaces. Such flows, however, tend to get modified, in case the opposite plates are sufficiently close to each other so that their respective EDLs overlap. In the present paper, closed form expressions are derived to depict the influence of the above phenomenon on ac electroosmotic flow patterns. It is seen that the EDL overlap has the most profound impact at lower ranges of frequencies, for which ions can equilibrate locally, and the bulk fluid behaves in a resistive manner, in case the applied potential is below the ionization potential so that electrolysis does not occur at electrode surfaces. The EDL formed, however, behaves in a capacitive manner. With EDL overlap, this capacitance increases (relative to the resistance), resulting in stronger potential gradients across the electrode surfaces. The present theory, thus, offers with a satisfactory explanation of ac electroosmotic fluid flow characteristics between parallel plate microelectrodes under overlapped EDL conditions. However, the present model does not take into account the variations of velocity magnitudes with conductivity, for which a non-linear analysis might be necessary.

Appendix A. Solution of the dynamic part of the electrical problem

The Fourier sine transform of the potential and charge density distribution can be written as:

$$\bar{\psi}(x,k) = \frac{2}{\pi}\int_0^\infty \psi(x,y)\sin(ky)\,dy, \tag{A.1}$$

$$\bar{\rho}_e(x,k) = \frac{2}{\pi}\int_0^\infty \rho_e(x,y)\sin(ky)\,dy. \tag{A.2}$$

This yields the following set of ordinary differential equations, from Eqs. (16) and (17):

$$\frac{\mathrm{d}^2\bar{\rho}_e}{\mathrm{d}x^2} = (1 + \mathrm{i}\omega + \delta^2 k^2)\bar{\rho}_e, \tag{A.3}$$

$$\frac{\mathrm{d}^2\bar{\psi}}{\mathrm{d}x^2} = \delta^2 k^2\bar{\psi} - \bar{\rho}_e. \tag{A.4}$$

In terms of the transformed variables, the boundary conditions (18a) and (18b) become (being attributed to the centerline symmetry)

$$\left.\begin{aligned} &\frac{\mathrm{d}}{\mathrm{d}x}(\bar{\rho}_e + \bar{\psi}) = 0 \\ &\psi = \frac{V_0}{\pi k} \end{aligned}\right\} \quad \text{at } x = 0, \tag{A.5}$$

$$\left.\begin{aligned} &\frac{\mathrm{d}\bar{\psi}}{\mathrm{d}x} = 0 \\ &\frac{\mathrm{d}\bar{\rho}_e}{\mathrm{d}x} = 0 \end{aligned}\right\} \quad \text{at } x = b. \tag{A.6}$$

Coupled with the boundary conditions given by Eqs. (A.5) and (A.6), Eqs. (A.3) and (A.4) can be solved to yield

$$\bar{\rho}_e = C_1\mathrm{e}^{ax} + C_2\mathrm{e}^{-ax}, \tag{A.7}$$

$$\bar{\psi} = C_3\mathrm{e}^{k\delta x} + C_4\mathrm{e}^{-k\delta x} - \frac{C_1}{1+\mathrm{i}\omega}\mathrm{e}^{ax} - \frac{C_2}{1+\mathrm{i}\omega}\mathrm{e}^{-ax} \tag{A.8}$$

where $a = \sqrt{1 + \mathrm{i}\omega + k^2\delta^2}$. Now, let

$$A = \frac{a}{k\delta}\frac{(e^{2ab}-1)iw}{(1-e^{2k\delta b})(1+iw)} - \frac{e^{2ab}+1}{(1+e^{2k\delta b})(1+iw)}.$$

Then, we have

$$\begin{aligned} C_1 &= \frac{V_0}{\pi k(1+e^{2k\delta b})A}, \\ C_2 &= C_1 e^{2ab}, \\ C_3 &= -C_1\frac{aiw}{k\delta}\frac{1-e^{2ab}}{(1+iw)(1-e^{2k\delta b})}, \\ C_4 &= C_3 e^{2k\delta b}. \end{aligned} \tag{A.9}$$

References

[1] N.G. Green, A. Ramos, A. Gonzalez, H. Morgan, A. Castellanos, Phys. Rev. E 61 (2000) 4011.
[2] N.G. Green, H. Morgan, J. Phys. D 30 (1997) 2626.
[3] M.P. Hughes, H. Morgan, F.J. Rixon, J.P.H. Burt, R. Pethig, Biochim. Biophys. Acta 1425 (1998) 119.
[4] M. Washizu, S. Suzuki, O. Kurosawa, T. Nishizaka, T. Shinohara, IEEE Trans. Ind. Appl. 30 (1994) 835.
[5] A. Gonzalez, A. Ramos, N.G. Green, A. Castellanos, H. Morgan, Phys. Rev. E 61 (2000) 4019.
[6] Q.-H. Wan, Analytical Chem. 69 (1997) 361.
[7] R.J. Hunter, Zeta Potential in Colloid Science, Academic, San Diego, 1981.
[8] J. Han, H.G. Craighead, Science 288 (2000) 1026.
[9] J. Li, et al., Nature (London) 412 (2001) 166.
[10] M.J. Levene, et al., Science 299 (2003) 682.
[11] L.R. Huang, E.C. Cox, R.H. Austin, J.C. Sturm, Science 304 (2004) 987.
[12] J.C.T. Eijkel, A. van den Berg, Microfluidics and Nanofluidics 1 (2005) 249.
[13] H. Daiguji, P. Yang, A.J. Szeri, A. Majumdar, Nano Lett. 4 (2004) 2315.
[14] W. Qu, D. Li, J. Colloid Interface Sci. 224 (2000) 397;
D. Li, Electrokinetics in Microfluidics, Elsevier, Amsterdam, 2004.
[15] R. Qiao, N.R. Aluru, J. Chem. Phys. 118 (2003) 4692.
[16] C. Lee, J. Zhou, T. George, F. Noca, American Physical Society, Division of Fluid Dynamics 56th Annual Meeting, November 23–25, 2003, East Rutherford, NJ, USA.
[17] F.H.J. van der Heyden, D. Stein, C. Dekker, Phys. Rev. Lett. 95 (2005) 116104.
[18] S.V. Patankar, Numerical Heat Transfer and Fluid Flow, Hemisphere/McGraw–Hill, 1980.